JACS
JOURNAL OF THE AMERICAN CHEMICAL SOCIETY
Article
pubs.acs.org/JACS

How Do Short Chain Nonionic Detergents Destabilize G-Protein-Coupled Receptors?

Sangbae Lee,[†] Allen Mao,[†] Supriyo Bhattacharya,[†] Nathan Robertson,[⊥] Reinhard Grisshammer,[‡] Christopher G. Tate,[*,§] and Nagarajan Vaidehi[*,†]

[†]Department of Molecular Immunology, Beckman Research Institute of the City of Hope, 1500 E. Duarte Road, Duarte, California 91010, United States

[⊥]Heptares Therapeutics Ltd, BioPark, Broadwater Road, Welwyn Garden City AL7 3AX, U.K.

[‡]Membrane Protein Structure Function Unit, National Institute of Neurological Disorders and Stroke, National Institutes of Health, Department of Health and Human Services, Rockville, Maryland 20852, United States

[§]MRC Laboratory of Molecular Biology, Cambridge Biomedical Campus, Francis Crick Avenue, Cambridge CB2 0QH, U.K.

Supporting Information

ABSTRACT: Stability of detergent-solubilized G-protein-coupled receptors (GPCRs) is crucial for their purification in a biologically relevant state, and it is well-known that short chain detergents such as octylglucoside are more denaturing than long chain detergents such as dodecylmaltoside. However, the molecular basis for this phenomenon is poorly understood. To gain insights into the mechanism of detergent destabilization of GPCRs, we used atomistic molecular dynamics simulations of thermostabilized adenosine receptor ($A_{2A}R$) mutants embedded in either a lipid bilayer or detergent micelles of alkylmaltosides and alkylglucosides. $A_{2A}R$ mutants in dodecylmaltoside or phospholipid showed low flexibility and good interhelical packing. In contrast, $A_{2A}R$ mutants in either octylglucoside or nonylglucoside showed decreased α-helicity in transmembrane regions, decreased α-helical packing, and the interpenetration of detergent molecules between transmembrane α-helices. This was not observed in octylglucoside containing phospholipid. Cholesteryl hemisuccinate in dodecylmaltoside increased the energetic stability of the receptor by wedging into crevices on the hydrophobic surface of $A_{2A}R$, increasing packing interactions within the receptor and stiffening the detergent micelle. The data suggest a three-stage process for the initial events in the destabilization of GPCRs by octylglucoside: (i) highly mobile detergent molecules form small micelles around the receptor; (ii) loss of α-helicity and decreased interhelical packing interactions in transmembrane regions are promoted by increased receptor thermal motion; (iii) transient separation of transmembrane helices allowed penetration of detergent molecules into the core of the receptor. The relative hydration of the headgroup and alkyl chain correlates with detergent harshness and suggests new avenues to develop milder versions of octylglucoside for receptor crystallization.

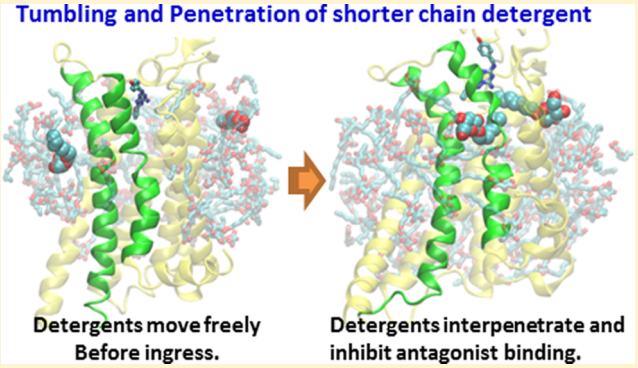

INTRODUCTION

The use of surfactants, also known as detergents, has a long history in the purification and crystallization of membrane proteins.[1−4] Initially, industrial detergents such as Triton X100 were the only ones available. These were a mixture of different aliphatic chain lengths, including short chain derivatives, and therefore these detergents often resulted in inactivation of membrane proteins, and they had limited utility for protein crystallization. With the development of chemically homogeneous detergents of different chemical structures, such as octylglucoside (OG) and lauryl-dimethylamine *N*-oxide (LDAO), it became possible to purify some membrane proteins[5,6] and, in the case of the bacterial photosynthetic reaction center and porins, to produce well-ordered crystals and determine the first atomic structures of membrane proteins.[7,8] However, it was appreciated even at this time that OG was a harsh detergent that often inactivated membrane proteins and that milder detergents were essential for working with most other membrane proteins.[9] The alkylmaltoside series has proven the most successful of these new detergents with the majority of bacterial transporters and ion channels being either purified or crystallized in dodecylmaltoside (DDM).[10] However, the shift of emphasis toward structure determination of mammalian membrane proteins highlighted that even DDM may not be mild enough for preserving their integrity upon solubilization and therefore even milder detergents were required.[11,12] Thus, there has been a continued effort to

Received: August 21, 2016
Published: October 28, 2016

DOI: 10.1021/jacs.6b08742
J. Am. Chem. Soc. 2016, 138, 15425−15433

develop novel mild detergents, including bicyclic alkylmaltosides,[13] bifacial amphiphiles[14] and maltose-neopentylglycols.[15]

Despite all the work to develop new detergents, the fundamental mechanism how nonionic detergents denature membrane proteins is unknown. The stability of any given membrane protein has evolved in the context of the biological membrane, where the protein has to be sufficiently stable to function and to confer a phenotype on the whole organism. Membrane proteins have not evolved to be stable in detergent micelles. This is not a fundamental limitation of the membrane protein, because many membrane proteins have been engineered through site-directed mutagenesis to be highly stable in detergent solution,[16] even in highly denaturing detergents such as sodium dodecyl sulfate.[17] Many reasons have been put forward for why detergents destabilize membrane proteins compared to lipids, although there is currently no accepted consensus.[18] Additionally, it is difficult to obtain molecular level insights into the mechanism of destabilization of membrane proteins in detergent micelles through experimentation.[19]

We have chosen to study the stability of G-protein-coupled receptors (GPCRs), a superfamily of seven helical transmembrane proteins, in detergent micelles using atomistic molecular dynamics (MD) simulations and thermostability measurements and have compared the results of the detergent simulations with those in a phosphatidylcholine (POPC) bilayer.

The properties of many different detergent micelles have been studied extensively by MD[20−27] and, more recently, simulations of ion channels and porins in detergent micelles have also been performed.[28−31] However, MD simulations have not been used to study the stability of GPCRs embedded in detergent micelles. The receptor we have used for this study, the human adenosine A_{2A} receptor ($A_{2A}R$), was chosen because its stability in lipid bilayers has already been thoroughly studied by MD simulations, both for the wild-type receptor and engineered thermostable mutant in different conformations.[32−34] In addition, there is a wealth of biochemical data on $A_{2A}R$ stability, in particular in different detergent solutions.[35−37] $A_{2A}R$ has been crystallized by a number of groups using three different strategies (thermostabilization,[38,39] T4 lysozyme fusion,[40,41] and antibody binding[42]) to facilitate the formation of well-ordered crystals. Structures have also been determined bound to a variety of different antagonists and agonists. The structures bound to an antagonist represent the inactive state of the receptor, whereas the agonist-bound structures represent an active-intermediate that has undergone substantial conformation changes.[38,39] Here we have studied the dynamics of $A_{2A}R$ in both the inactive and active-intermediate states. The microsecond time scale available for these studies is insufficient to observe the full denaturation process of a receptor, but we found this was sufficient to observe the substantial differences between the effects of long chain and short chain detergents on the structure of $A_{2A}R$ mutants.

RESULTS

Before studying the $A_{2A}R$ mutants in detergent micelles, we used MD simulations to assemble the micelles of four detergents, *n*-dodecyl-*β*-D-maltoside (DDM), *n*-decyl-*β*-D-maltoside (DM), *n*-nonyl-*β*-D-glucoside (NG), and n-octyl-*β*-D-glucoside (OG), in the absence of protein to test the validity of our simulations (see Methods). Following an aggregated 500 ns MD simulation on each micelle, the micelles of all the detergents assembled into an oblate spheroid, as previously observed for DDM.[20,43,44] The radius of gyration and the eccentricity of each micelle (Supplemental Table S1) were found to compare well with small angle X-ray scattering (SAXS) measurements for these micelles.[45] The agreement between the MD simulations and the experimental data for the shape and size of the micelle particles shows that the simulations recapitulated the experimental properties of the detergent micelles.

Two structures of $A_{2A}R$ were chosen for the MD simulations in detergent, namely, $A_{2A}R$-StaR2[39] with the antagonist ZM241385 bound (PDB code 3PWH) and $A_{2A}R$-GL31[38] with the agonist adenosine bound (PDB code 2YDO). Both of the $A_{2A}R$ mutants contain thermostabilizing mutations (see Methods) that stabilize the inactive R state for $A_{2A}R$-StaR2[35] and the active-intermediate R′ state for $A_{2A}R$-GL31.[36] Each of the receptors was first assembled into a detergent micelle containing either 192 molecules of DDM, 144 molecules of DM, 155 molecules of NG, or 123 molecules of OG. These values are larger than the aggregation number for the pure detergent and reflect the total number of detergent molecules specifically bound to membrane proteins determined from biochemical assays.[46−50] As expected, the radius of gyration and the eccentricity of each protein−detergent micelle are larger than those for the pure detergent (Supplementary Table S1). After assembly, each receptor embedded in detergent was subjected to a further five simulations, 100 ns each, and a representative structure of the most populated conformation ensemble was determined (Figure 1). After completion of the simulations, a series of analyses were performed on both the detergent and receptor for each of the detergents studied.

Characteristics of the Detergent Micelle around $A_{2A}R$-StaR2. The distribution of detergent molecules in the micelles around $A_{2A}R$-StaR2 differed dependent upon the detergent type. For DDM and DM, there was a higher probability of the hydrophobic aliphatic "tail" being closer to the receptor than the hydrophilic maltoside "headgroup", as shown by the radial distribution function (Figure 2). Thus, the number density of tail groups of DDM and DM around $A_{2A}R$-StaR2, peaks at 18 and 20 Å from the receptor core, respectively, while the distance of their head groups peaks at 27 and 32 Å, respectively. In contrast, there was no significant difference between the distribution of the tail and headgroups of the short chain detergents (Figure 2). This substantiates visual inspection of representative $A_{2A}R$-StaR2−detergent micelle structures where the micellar surface composed of DDM and DM has a greater density of hydrophilic groups on the outer surface of the micelles compared to the micelles of NG or OG (Figure 1 and Figure S1). Additionally, the rate of movement of detergent molecules within the micelle showed substantial difference between the long chain and short chain detergent micelles. For DDM or DM, individual detergent molecules diffuse relatively slowly, and thus the position of a given molecule varies little with time (Figure 2 and Figure S2). In contrast, molecules of NG and OG diffuse rapidly, often with the detergent tumbling within the micelle, allowing it to sometimes sample the whole space of the micelle within the length of the simulation. Another difference between the long chain and short chain detergents is that on a number of occasions OG molecules were observed to penetrate into the receptor core (Supplementary movie; discussed further below). Tumbling or penetration of DDM or DM into $A_{2A}R$-StaR2 was not observed.

DOI: 10.1021/jacs.6b08742
J. Am. Chem. Soc. 2016, 138, 15425−15433

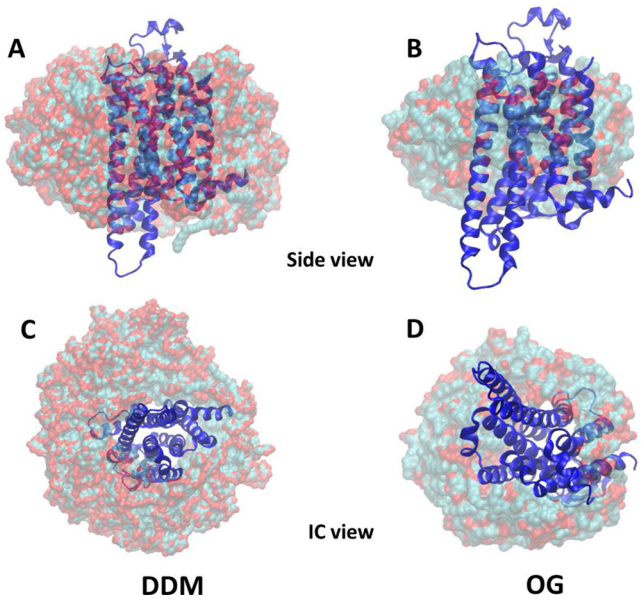

Figure 1. Representative structures from the most populated MD conformation ensemble of A_{2A}R-StaR2 in the detergents DDM (A and C) and OG (B and D). Atoms in detergent are depicted as spheres (hydrophilic atoms as red; hydrophobic atoms as cyan), and the receptor is shown in cartoon representation (dark blue). The A_{2A}R-StaR2−detergent micelle complexes are shown in the two different views, equivalent to either parallel to the membrane plane (side view; A and B) and viewed from the intracellular (IC) surface (C and D). See Supporting Information (Figure S1) for data on simulations in DM and NG.

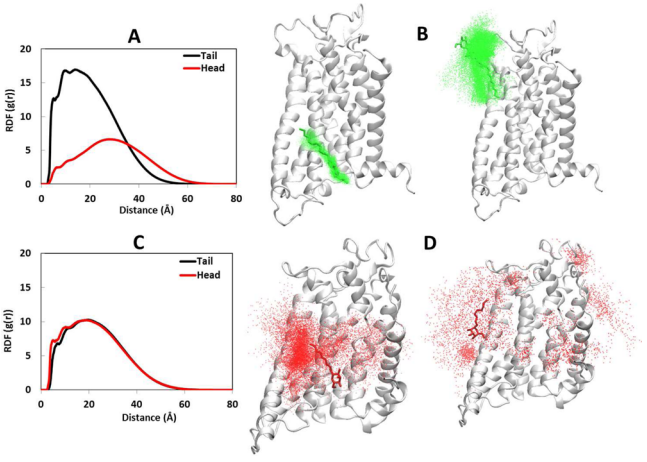

Figure 2. OG is highly mobile in the A_{2A}R-StaR2−detergent complexes compared to DDM. The radial distribution function (RDF) gives the density for either the headgroup or tail-group of the detergents as a function of distance from the center of mass of A_{2A}R-StaR2 in DDM (A) and OG (C); tail group, black curve; headgroup, red curve. (B and D) Spatial distribution plots of two representative detergent molecules for DDM (B) and OG (D) within 6 Å of A_{2A}R-StaR2 from the most populated ensemble. The initial position of the detergent molecules is shown in stick representation and the resultant spatial distributions are shown as dots; green, DDM, and red, OG). See Supporting Information (Figure S2) for data on simulations in DM and NG.

The Structure and Stability of Receptor−Detergent Complexes in Different Detergents. To validate the MD simulations of the receptors, we compared experimentally determined apparent T_m determinations[35] with the average potential energy of the receptor conformations calculated over the entire MD trajectory (Figure 3). The good correlation

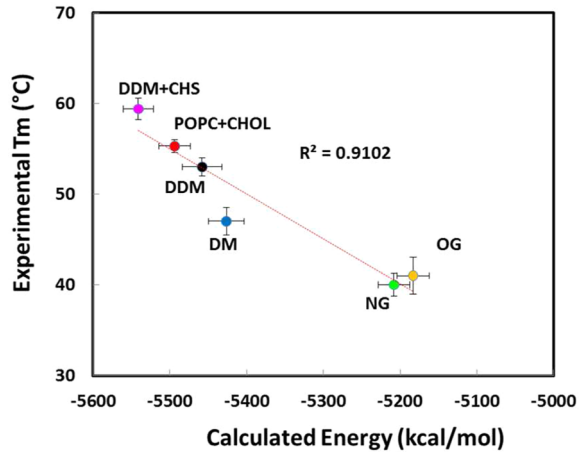

Figure 3. Comparison of the calculated potential energy of A_{2A}R-StaR2 in different environments with apparent T_m values determined experimentally. The apparent T_m of A_{2A}R-StaR2 was determined using a radioligand-based thermostability assay[31] and plotted against the potential energies calculated from the MD simulations. Experimental T_m for comparisons to detergent simulations were determined from purified receptors in the detergents stated. For the comparison with the simulations performed in POPC + cholesterol, the receptors were assayed in insect cell membranes. Magenta, DDM + CHS; red, POPC + CHOL; black, DDM; blue, DM; green, NG; orange, OG. The best fit line was determined by linear regression, and error represents standard deviation (sd).

between the experimental data and the computational data suggests that MD simulations are good models for understanding the stability of GPCRs in both detergents and membranes. Interestingly, the highest stability for A_{2A}R-StaR2 was observed for the receptor solubilized in DDM supplemented with cholesteryl hemisuccinate (CHS), followed by receptor embedded in membranes. DDM was the best detergent to stabilize A_{2A}R-StaR2, closely followed by DM, but both NG and OG destabilized the receptor significantly. The average potential energy is the sum of the internal energy of the receptor and the interaction energy of the receptor with the detergent or palmitoyloleoylphosphatidylcholine, (POPC), cholesterol (wherever applicable), and water molecules. The difference in the stability of A_{2A}R-StaR2 in various detergents comes predominantly from the receptor−detergent interaction energies and the non-bond energy of the receptor (Figure S3). This could arise due to the more frequent interaction of the hydrophobic portions of DDM and DM with the receptor with respect to their head groups, compared to NG and OG where there is an equal probability of head groups or tails interacting with the hydrophobic portions of the receptor. In addition, the larger micelle size of DDM and DM more effectively shields the hydrophobic portions of the receptor compared to NG and OG. This is reflected in the higher hydrophobic solvent accessible surface area (SASA) of A_{2A}R in OG compared to DDM (Figure S4).

What are the consequences on the receptor structure when the receptor is inserted into a detergent micelle that is destabilizing?

Variations in the structure of A_{2A}R-StaR2 observed in the MD trajectories were clustered based on two properties that

DOI: 10.1021/jacs.6b08742
J. Am. Chem. Soc. 2016, 138, 15425−15433

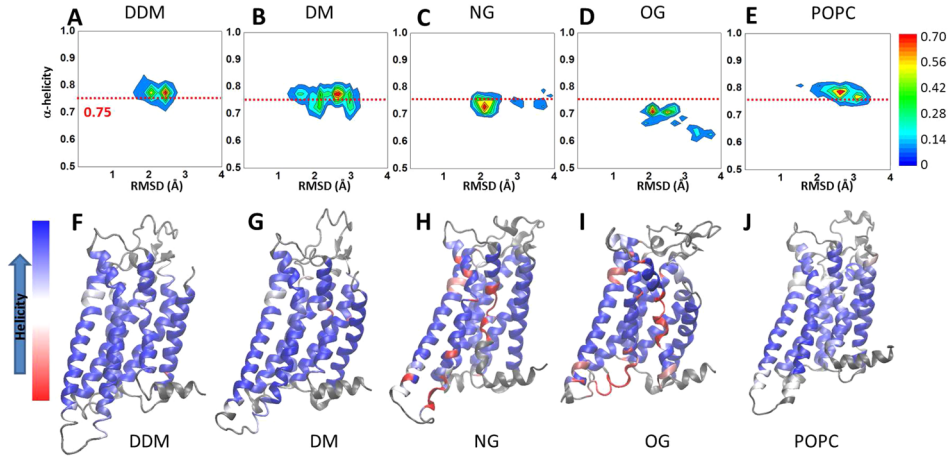

Figure 4. Structural heterogeneity of A_{2A}R-StaR2 in various detergents and in a POPC. (A–E) Population distributions of A_{2A}R-StaR2 are depicted in relation to helical content and RMSD in coordinates from the respective crystal structures. Simulations of A_{2A}R-StaR2 (PDB code 3PWH) were performed in the following environments: (A) DDM; (B) DM; (C) NG; (D) OG; (E) POPC. The red-dotted lines in the figure are the α-helical content of the crystal structure of A_{2A}R-StaR2. Representative structures extracted from the most populated ensemble of A_{2A}R-StaR2 in the following detergents or lipid are shown: (F) DDM; (G) DM; (H) NG; (I) OG; (J) POPC. The color scheme ranges from blue to red, with red indicating the lowest helicity in the TM regions. Loop regions are not included in this analysis and are colored dark gray. The percentages of snapshots represented by these structures within the most populated cluster indicated by the red regions are 45% (DDM), 36% (DM), 24% (NG), 29% (OG), and 48% (POPC). Inclusion of MD structures from the yellow regions increases the population to 68% (POPC), 69% (DDM), 40% (NG) and 43% (OG).

measured the structural deviation from the crystal structure, namely, the root-mean-square deviation (RMSD) in the coordinates of the backbone atoms and the percentage α-helicity of residues in the transmembrane (TM) helices (Figure 4). Both DDM and POPC maintain A_{2A}R-StaR2 in a state similar to the crystal structure, although there is greater flexibility of the receptor in the lipid bilayer compared to that in a DDM micelle (Figure 4). However, it is noticeable that the harsher the detergent, the greater the deviation from the crystal structure and the lower the α-helicity of the transmembrane regions (Figure S5). This is particularly apparent for A_{2A}R-StaR2 in either OG or NG where there are significant perturbations in the middle of TM7, the cytoplasmic end of TM6, and the loop regions. Each of the transmembrane regions in A_{2A}R-StaR2 maintains a stable α-helix in DDM and DM simulations, but TM5, TM6, and TM7 show relatively low helicity (50–70%) in OG.

The alterations in secondary structure are also reflected in the decrease in the average number of interhelical hydrogen bonds and van der Waals interactions (Figure S6). A_{2A}R-StaR2 in DDM has the highest number of interhelical interactions (61 contacts) with the lowest number of interhelical interactions in OG (48 contacts). The greater flexibility of A_{2A}R-StaR2 in OG has a secondary consequence, because as the transmembrane helices move apart, then it is possible for a detergent molecule to intercalate between them. Out of five 100 ns simulations of A_{2A}R-StaR2 in OG, signification penetration of the α-helical bundle was observed on three occasions (Figure 5; Online movie file 1). The remaining two simulations that did not show penetration of OG within 100 ns simulation time showed penetration when the simulations were extended to 200 ns each. In all these simulations, the OG molecule entered the receptor through TM6 and TM7 (see Figure S7). In one example, the antagonist ZM241385 is also displaced from its normal binding position in the orthosteric binding pocket, suggesting that OG could inhibit antagonist binding. However, it is also likely that further ingressions of OG into the core of the receptor could lead to further unfolding and ultimately to

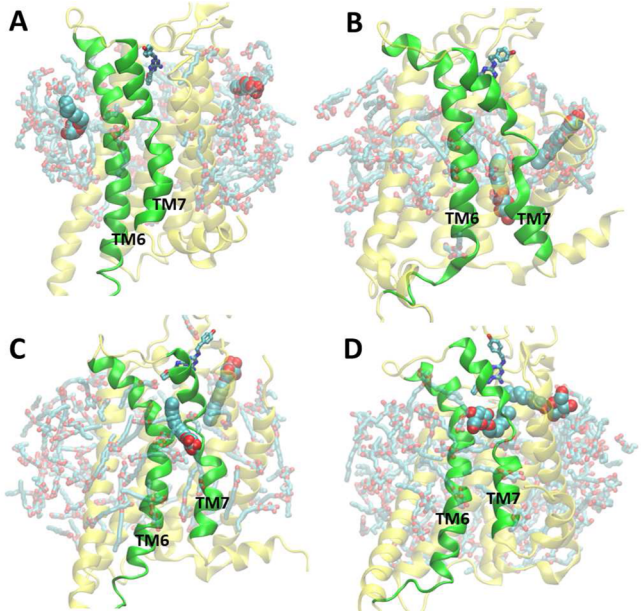

Figure 5. Loss of structural integrity of A_{2A}R-StaR2 in OG. Panels show a series of snap shots of A_{2A}R-StaR2 in OG using the same view of the receptor during a 100 ns simulation. (A) Starting state: before ingress, detergents move freely and diffuse rapidly with tumbling within micelle. (B) Separation of adjacent α-helices (38 ns): Helices move; no ingress. TM6 and TM7 start unraveling. (C) Intermediate state in the penetration process (64 ns): Start of ingress. Detergent is starting penetration between TM6 and TM7. (D) Final state: Detergents interpenetrate and inhibit antagonist binding, so ZM241385 (stick model) is displaced off from normal binding site.

complete denaturation, which is the outcome of trying to solubilize and purify A_{2A}R-StaR2 in OG (which is on a significantly longer time scale than the simulations). To eliminate the possibility that the tumbling and penetration of the OG molecules are not arising due to smaller micelle size (123 molecules) compared to DDM, we performed the OG

DOI: 10.1021/jacs.6b08742
J. Am. Chem. Soc. 2016, 138, 15425–15433

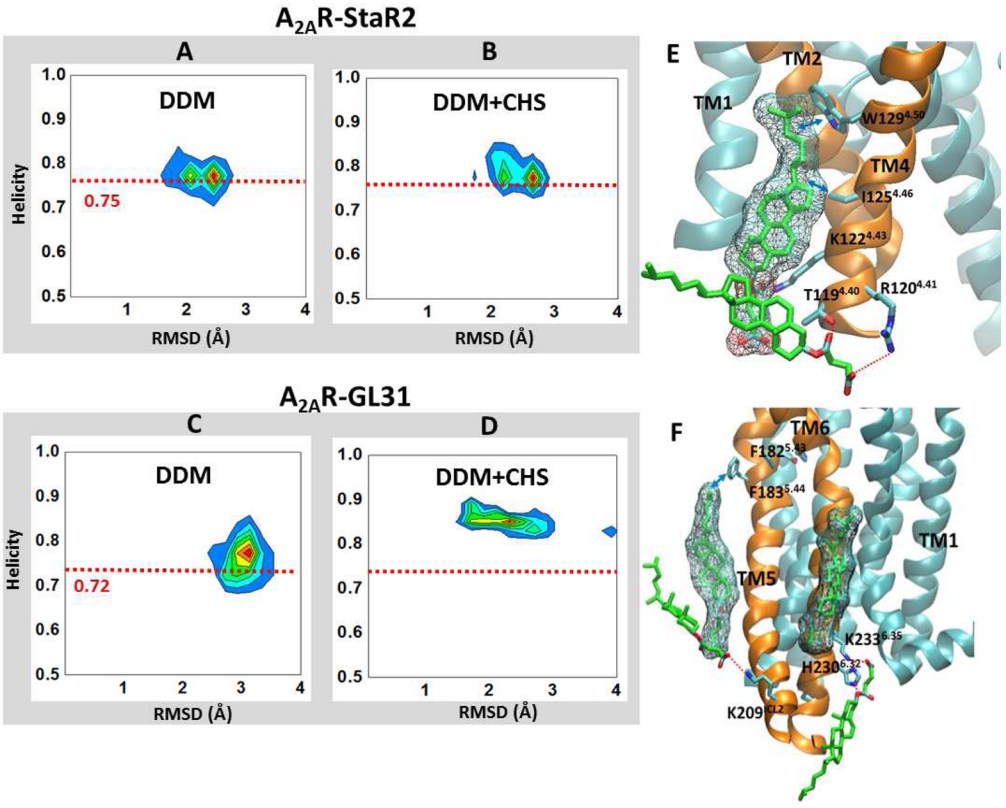

Figure 6. Selective stabilization of A_{2A}R-GL31 compared to A_{2A}R-StaR2 by CHS. The effect of CHS on the distributions of the conformational ensembles is depicted with respect to helicity and RMSD from the crystal structure of the respective receptors. (A and B) A_{2A}R-StaR2 (antagonist conformation); (C and D), A_{2A}R-GL31 (active-intermediate conformation). (E and F) CHS interaction sites identified from the MD simulations of A_{2A}R-GL31. Panel E shows representative snapshots from the MD simulations showing the residues in TM4 that make close contact with CHS. Two residues, 4.46 and 4.50, have also shown to be important in cholesterol binding in the crystal structure of β_2-adrenergic receptor (PDB code 3D4S). The hydrogen bonds between headgroup of CHS and the residues are shown as red-dotted lines, and hydrophobic interactions of the tail of CHS and the residues are shown as blue arrows. In panel F, the headgroup of CHS makes strong hydrogen bonds with residues H230$^{6.32}$ and K233$^{6.35}$. The effect of cholesterol on the conformational ensemble in the POPC bilayer is depicted in the Supporting Information (Figure S10).

micelle simulations starting with 192 OG molecules similar to the number of detergents in the DDM micelle. The OG molecules in these simulations showed tumbling in the micelle and penetration into the receptor that confirmed that this phenomenon is characteristic of the short chain detergents (see Figure S8).

Stabilizing Membrane Proteins with Either Ligands, Cholesteryl Hemisuccinate, or Lipids. In experimental systems, the stability of a GPCR is crucial for subsequent success in its purification and crystallization. The first step of the process is to perform high-throughput detergent screening to identify those detergents that maintain the protein in a monodisperse and functional state.[51,52] It is well-known that adding either ligands[53] or lipids[54] can improve the stability of a membrane protein in detergent. So for example, ZM241385 binding to A_{2A}R improves its stability,[37,39] as does the binding of agonists to A_{2A}R-GL31.[37,38] Simulations suggested that in both cases, adding a ligand improved the helicity and decreased the flexibility for both A_{2A}R-StaR2 and A_{2A}R-GL31 (Figure S9A,B), which correlates with the increase in number of interhelical packing interactions (Figure S9C). Cholesteryl hemisuccinate (CHS) is another factor that is known to improve the stability of A_{2A}R in DDM.[37,55] Indeed, it is not possible to purify A_{2A}R in DDM unless CHS is added to each step of the procedure,[55] although once the protein has been thermostabilized in the inactive state (A_{2A}R-StaR2) CHS is no longer required to maintain functionality during purification.[35] Simulations of A_{2A}R-StaR2 in DDM supplemented with CHS did not show any significant difference in its flexibility compared to the receptor in DDM alone (Figure 6). In contrast, simulations of A_{2A}R-GL31 in DDM supplemented with CHS showed an appreciable increase in α-helicity and a decrease in RMSD compared to the crystallized receptor after MD simulations (Figure 6A–D); this effect was also observed in simulations of the receptors in a POPC lipid bilayer with cholesterol (Figure S10A). The basis for the stabilizing effect of CHS appears to be its interaction with A_{2A}R-GL31 with TM4. In addition, interactions between CHS and residues N181$^{5.42}$ and A184$^{5.45}$ on TM5 and H230$^{6.32}$ and K233$^{6.35}$ on TM6 stabilizes these helices (Figure 6E,F). This is the same site where CHS resides in some of the crystal structures of the β_1-adrenergic receptor[56] and the β_2-adrenergic receptor,[57,58] although all the residue contacts in the crystal structures are not captured in the MD simulations.

The presence of phospholipids in a detergent micelle is another factor that is known from experimentation to improve the stability of many membrane proteins.[59] This can be specific to a particular lipid or it can be a more general effect that can be effected by many different lipids. To observe the effects of lipids on the stability of A_{2A}R-StaR2, simulations were performed where an annular layer of POPC lipids surrounded the receptor in an OG micelle.

DOI: 10.1021/jacs.6b08742
J. Am. Chem. Soc. 2016, 138, 15425–15433

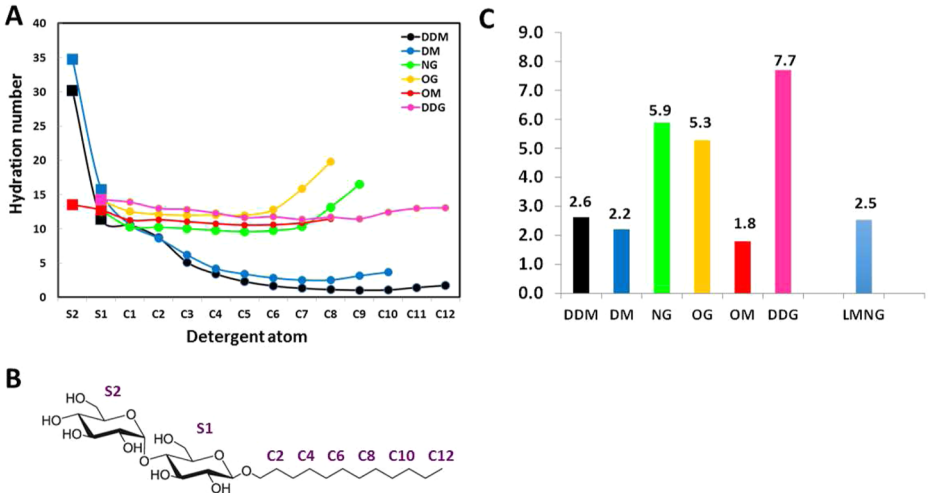

Figure 7. Relative hydration of detergents in solution. (A) Hydration numbers for the sugar head groups and alkyl chains of detergents. The hydration number is the average number of waters near each organic moiety in the detergent during the MD simulations. In each case, these have been determined by radial distribution functions between each carbon atom in the alkyl chain and the center-of-mass of sugar rings in the headgroup, to the oxygen atoms of water molecules within 5.0 Å of the detergent. Hydration number profiles for DDM, DM, NG, OG, OM, and dodecyl β-D-glucopyranoside (DDG) are colored in black, blue, green, orange, red, and purple, respectively. *B*. Nomenclature for panel A shown on a model of DDM. (C) The ratio of hydration numbers (RHN) for each detergent was calculated from the ratio of the summation of average hydration number for the alkyl chain ($\bar{C}_i$ is the average hydration number for carbon in the alkyl chain) to the summation of average hydration number of the headgroup ($\bar{S}_i$), as follows.

$$\mathrm{RHN} = \left(\frac{\sum_{i=1}^{j} \bar{C}_i}{\sum_{i=1}^{j} \bar{S}_i} \right)$$

In contrast to the receptor in pure OG micelles, the $A_{2A}R$-StaR2 is less flexible in the OG micelle when surrounded by a POPC annular layer, and OG shows no penetration into the receptor (Online movie file 2). The OG molecules tumble and displace the POPC molecules from the vicinity of the receptor (Figure S11). However, the alkyl chains of the lipid POPC molecules point to the hydrophobic regions of the TM helices of the receptor as shown by the decrease in the hydrophobic solvent accessible surface area (Table S2) and increase in the stability of the receptor compared to just the OG micelle (see Figure S3).

DISCUSSION

The stability of membrane proteins in detergent is a key parameter that dictates the probability of success in their purification, crystallization, and structure determination.[12,60] Despite this, there is little understanding of how detergents destabilize membrane proteins or how adding lipids can stabilize them. Here we show that MD simulations can perhaps offer some insights into some of the initial molecular events that could destabilize different conformations of $A_{2A}R$. The simulations of $A_{2A}R$ in the harsh detergent OG showed that the detergent was highly mobile and formed a micelle around the receptor with no discernible difference in hydrophobicity between the region around the hydrophobic core of the receptor and its surface. Addition of POPC annular lipid layer stabilized the receptor in the OG micelle by covering the receptor hydrophobic region of the TM helices.

In contrast, simulations of $A_{2A}R$ in the mild detergent DDM showed that the detergent was not very mobile and formed a micelle around the receptor that showed high hydrophobicity in its interior and low hydrophobicity on the exterior. Thus, DDM mimics the hydrophobic environment of the membrane better than OG, and the corresponding interhelical contacts within $A_{2A}R$ are better preserved in DDM than in OG. It is well-known that the addition of CHS or ligands can stabilize membrane proteins upon detergent solubilization. MD simulations suggest that ligands stabilize interhelical interactions within $A_{2A}R$, while CHS interacts directly with the receptor, reducing the flexibility in the transmembrane helices and thereby improving the stability of the receptor. The simulations offer only a hint of some of the processes that may occur in a receptor−detergent micelle, because the time scale of the all-atom MD simulations (100 ns) is several orders of magnitude smaller than the time scale for the purification of a membrane protein (hours to days). Thus, the ultimate result of adding a harsh detergent to an unstable receptor, which is receptor aggregation and precipitation, was not observed. However, in three out of five simulations, it was observed that OG molecules interpenetrated between transmembrane domains and could even displace the bound antagonist ZM241385, which binds with nanomolar affinity to $A_{2A}R$.[61] This appears to be a consequence of the significantly increased dynamics of $A_{2A}R$ in OG compared to DDM, because OG ingress into the receptor always followed the separation of two adjacent α-helices. In DDM, where $A_{2A}R$ is far less dynamic, no interpenetration of detergent into the receptor was observed, regardless of the conformation of the receptor. This hints at the possibility that breaking interhelical interactions and the partitioning of the detergent into the receptor could be initial steps in the inactivation process, which leads ultimately to irreversible denaturation.

Both OG and NG appear to have a significant advantage for membrane protein crystallography, because the size of the micelle they form around a small membrane protein is less

DOI: 10.1021/jacs.6b08742
J. Am. Chem. Soc. 2016, 138, 15425−15433

likely to occlude hydrophilic loops essential for the formation of crystal contacts.[62,63] It is noteworthy that so far, GPCRs whose structures have been determined in the absence of either antibodies, nanobodies, or T4 lysozyme fusions have been crystallized in NG, OG, or hega-10 or in the lipidic cubic phase.[38,56,64] No structures have been determined from receptors crystallized in either DDM, DM, or lauryl maltose neopentyl glycol (LMNG), presumably due to the large size of the detergent occluding hydrophilic surfaces and preventing close associations necessary for crystal lattice formation. Of course, the significant disadvantage of OG and NG is that they are so harsh that they rapidly denature most mammalian membrane proteins. This raises the interesting question of whether the MD simulations offer any insight into routes to design new detergents that have the size of OG or NG but the mildness of DM or DDM. The major difference observed in the behavior of DDM and OG during the MD simulations was the rate of tumbling and diffusion within the micelle. Intuitively, this could be a reflection on the relative hydrophobicity of the alkyl chain and the sugar headgroup, previously referred to as the hydrophile−lipophile balance (HLB).[65] Here we have calculated a more pertinent parameter for alkyl maltosides and glucosides that takes into account the degree of hydration of the headgroup compared to the hydration of the alkyl chain during the MD simulations. This ratio of hydration numbers (RHN; hydration number for the tail group divided by the hydration number for the tail group) gives large values for the alkyl glucosides (OG, NG, and DDG; harsh detergents) and small numbers for the alkyl maltosides (OM, DM, DDM, and LMNG; mild detergents) (Figure 7). The prediction is therefore that decreasing the RHN ratio of OG by increasing the hydrophilicity of the headgroup of OG would result in a milder detergent, as is observed for OM (the interhelical packing interactions of A_{2A}R-StaR2 in OM detergent are close to those in DM detergent) (Figure S12). MD simulations of novel detergents will offer an attractive route to testing these *in silico* before embarking on their synthesis, assaying their biophysical properties, and finally seeing whether they do, indeed, maintain membrane proteins in a biologically relevant conformation for a sufficient length of time to allow crystallization and structure determination.

METHODS

Receptor Preparation. All the MD simulations were performed using the GROMACS package[66] with the GROMOS force field.[67] The initial coordinates of A_{2A}R-GL31 and A_{2A}R-StaR2, including the coordinates of the agonist adenosine and antagonist ZM241385, were taken from the PDB file with the PDB codes 2YDO[38] and 3PWH,[39] respectively. The antagonist ZM241385 bound A_{2A}R-StaR2 thermostable mutant (PDB code 3PWH) in the inactive state contains eight mutations at positions A54L$^{2.52}$, T88A$^{3.36}$, R107A$^{3.55}$, K122A$^{4.43}$, L202A$^{5.63}$, L235A$^{6.37}$, V239A$^{6.41}$, and S277A$^{7.42}$.[37] The Ballesteros−Weinstein amino acid numbering system designations used for class A GPCRs are shown as superscripts.[68] The agonist adenosine bound active-like state mutant A_{2A}R-GL31 (PDB code 2YDO) has four mutations, L48A$^{2.46}$, A54L$^{2.52}$, T65A$^{2.63}$, and Q89A$^{3.37}$.[38] We performed MD simulations for both A_{2A}R-StaR2 and A_{2A}R-GL31 with and without their respective antagonist and agonist ligands bound.

Building and Optimizing Micelle Structures. The number of detergent molecules per micelle was chosen to be larger than the aggregation number of each detergent studied here. We used 192 DDM molecules, 144 DM, 155 NG, and 123 OG molecules to build their respective micelles. The aggregation numbers for these detergents are given in Table S1. The hydrophobic region of the GPCR, which is cylindrical in shape, was estimated to be 60 Å, from the range of the minimum and maximum of the Z coordinates of the heavy atoms (see Figure S13). The radius of the GPCR is estimated to be 30 Å as shown in Figure S13. Based on this estimated size, the hydrophobic tail of the detergents would reside in 20 Å ring like sections around the hydrophobic middle of the GPCR cylinder. We divided the micelle into six ring sections spaced 3.3 Å apart. Also the six rings would be able to accommodate 32 methyl groups found at the end of the detergent tail. For example, this geometrical constructs resulted in accommodating 192 DDM molecules close to the aggregation number of DDM (~200). The first step was to create four pseudoatom points that would represent the ideal spacing and packing for each detergent molecule. For example, for the DDM molecule, the pseudoatom point 1 was chosen at the end of the hydrophobic tail of DDM, point 2 was the in the middle of the hydrophobic tail, points 3 and 4 were in the headgroup (see Figure S13). These points were used to place all the DDM molecules in the same orientation. For the 192 DDM molecules, x, y, and z coordinates for all points were calculated to maximize spacing between each detergent molecule. A transformation matrix between the original coordinates of the detergent molecules and the new array using the four pseudoatom points was calculated for each of the 192 DDM molecules and applied to generate new coordinate files for the detergent molecules. The internal conformations of the detergent molecules were taken from the protein structure database. The same procedure was repeated for DM, NG, and OG with the same six ring sections, and spacing changed based on the number of molecules, 144, 150, and 120, respectively. The chemical structures of the detergents used in this study are shown in Figure S14, and the starting micelle particles are shown in Figure S13B.

Building of the Receptor−Micelle Complexes. The A_{2A}R-GL31/StaR2 receptor was inserted into each of the four detergent micelles built as described above. The receptor−detergent complex was constructed by inserting the receptor into hollow micelles. The detergent molecules were placed randomly with the terminal alkyl (methyl) groups of their tails at a minimum distance of 4 Å from the receptor exterior to avoid steric clashes. Each detergent headgroup was placed approximately equidistant from its nearest neighbors. After energy minimization of this system, the receptor−micelle system was solvated with waters[69] by superimposing a box of water followed by removal of water molecules that were too close to the receptor (within 4 Å of receptor). We used the SPC force field for describing the waters.[69] Chloride ions were added to the systems as the counterions for neutralizing the whole system. In the DDM simulation with CHS, the DDM molecules were randomly replaced with 25 CHS molecules in keeping with the concentration ratio (w/w) of CHS to DDM used in experiments namely, 0.1% DDM to 0.01% CHS.[70,71] The receptor−micelle complexes were equilibrated using MD simulations as described in the next section. The resulting receptor−detergent micelle complexes had 6003 atoms in OG to 11 115 atoms in DDM for simulations.

Details of MD Simulations. We used the GROMACS v4.6 to perform all the MD simulations in this study. The MD simulations were performed at 300 K. Solvent and solute (receptor−detergent system) were independently coupled to a temperature bath with a relaxation time of 0.1 ps.[72] The pressure was calculated using a molecular virial and held constant by weak coupling to a pressure bath with a relaxation time of 0.5 ps. For all the equilibration simulations, the receptor was positionally restrained, and the simulations were performed at constant volume (NVT). Thus, no pressure coupling was applied in these cases. Bond lengths and the geometry of the water molecules were constrained using the SHAKE algorithm.[73] The equations of motion were integrated using the leapfrog algorithm and a time step of 2 fs. Center of mass motion was removed every 20 fs. The short-range van der Waals and electrostatic interactions were evaluated at every time step by using a charge-group pair list with cutoff radius of 8 Å between the centers of geometry of the charge groups. Longer-range van der Waals and electrostatic interactions, between pairs at a distance longer than 8 Å and shorter than a long-range cutoff of 14 Å, were evaluated every fifth time step, at which point the pair list was also updated, and were kept unchanged between

DOI: 10.1021/jacs.6b08742
J. Am. Chem. Soc. 2016, 138, 15425−15433

these updates. For equilibration of the receptor−detergent complexes, the atoms of the protein were positionally restrained using a harmonic restraining force with a force constant of 1000 kJ/(mol·nm) during the 200 ps of equilibration. In this step, the water molecules and detergent were movable to optimize their packing around the receptor. The system was further equilibrated using NPT ensemble, while the force constant of the restraining force was set to 5 kcal/mol and reduced to zero stepwise at each 2 ns. At this point, the pressure coupling was switched on. This results in a total equilibration time of 10 ns. We performed an additional 5 ns of simulations without restraints before the production runs. Five independent simulations each to 100 ns were performed with different starting velocities. The analyses of the convergence of the five simulation runs, along with the energy analysis are discussed in the Supporting Information. The average representative structures from MD simulations were calculated as follows. We performed conformation clustering using RMSD cutoff of 1.2 Å on the concatenated MD simulation trajectories from the five simulations for any given system. The most representative structure of the most populated cluster was calculated as the frame that has the smallest RSMD to the center of this cluster of conformations.

Building of the Receptor−Bilayer Complexes and MD Simulations in a Bilayer. The starting conformations of $A_{2A}R$ were taken from the crystal structures of GL31 and StaR2 (PDB codes 2YDO for GL31 and 3PWH for StaR2). The structures were solvated in SPC water and explicit lipid (palmitoyloleoylphosphatidylcholine, POPC) using the *inflategro* package in GROMACS.[66] We performed the MD simulations on $A_{2A}R$ in a POPC bilayer lipid using PBC (periodic boundary conditions) with GROMOS96 force field.[74] We used SETTLE[75] and LINCS[76] algorithm for the bond and angle for water and all other bonds with a 2 fs time step. A 12 Å cutoff distance was used for nonbonded interactions, and the coordinates were saved every 2 ps for analysis. In addition, we used the PME (particle mesh Ewald) method[77,78] for long-range van der Waals interaction. Each system was equilibrated for 200 ps at 310 K using a NVT ensemble followed by 10 ns of MD under constant pressure, NPT condition with a pressure of 1 bar. In this stage, receptor and ligand were kept in place using position restraints. After NPT equilibration, we performed a total of 10 production runs for a total of 100 ns with different velocities using the constant volume, NVT ensemble. Additional details are provided in the SI (Supporting Information) text.

■ ASSOCIATED CONTENT

Supporting Information

The Supporting Information is available free of charge on the ACS Publications website at DOI: 10.1021/jacs.6b08742.

Details on data sets for molecular dynamics along with supporting figures, tables, and descriptions of the videos (PDF)

Video of OG micelle showing greater mobility with a tumbling effect of the detergents within the micelle (MPG)

Video of simulation of $A_{2A}R$-StaR2 in an OG micelle when the receptor surface is covered by an annular layer of POPC lipid bilayer (MPG)

■ AUTHOR INFORMATION

Corresponding Authors

*cgt@mrc-lmb.cam.ac.uk

*NVaidehi@coh.org

Notes

The authors declare no competing financial interest.

■ ACKNOWLEDGMENTS

This work was funded by NIH Grant R01-GM097261 to N.V. Work on GPCRs in C.G.T.'s lab is funded by the Medical Research Council (MC_U105197215) and an ERC Advanced Grant (EMPSI 339995). R.G. is supported by the Intramural Research Program of the National Institutes of Health, National Institute of Neurological Disorders and Stroke.

■ REFERENCES

(1) le Maire, M.; Champeil, P.; Møller, J. V. *Biochim. Biophys. Acta, Biomembr.* **2000**, *1508*, 86.

(2) Prive, G. G. *Methods* **2007**, *41*, 388.

(3) Helenius, A.; Simons, K. *Biochim. Biophys. Acta, Rev. Biomembr.* **1975**, *415*, 29.

(4) Garavito, R. M.; Ferguson-Miller, S. *J. Biol. Chem.* **2001**, *276*, 32403.

(5) Michel, H. *J. Mol. Biol.* **1982**, *158*, 567.

(6) Garavito, R. M.; Jenkins, J.; Jansonius, J. N.; Karlsson, R.; Rosenbusch, J. P. *J. Mol. Biol.* **1983**, *164*, 313.

(7) Deisenhofer, J.; Epp, O.; Miki, K.; Huber, R.; Michel, H. *Nature* **1985**, *318*, 618.

(8) Cowan, S. W.; Schirmer, T.; Rummel, G.; Steiert, M.; Ghosh, R.; Pauptit, R. A.; Jansonius, J. N.; Rosenbusch, J. P. *Nature* **1992**, *358*, 727.

(9) Deisenhofer, J.; Michel, H. *EMBO J.* **1989**, *8*, 2149.

(10) Parker, J. L.; Newstead, S. *Protein Sci.* **2012**, *21*, 1358.

(11) Sonoda, Y.; Newstead, S.; Hu, N. J.; Alguel, Y.; Nji, E.; Beis, K.; Yashiro, S.; Lee, C.; Leung, J.; Cameron, A. D.; Byrne, B.; Iwata, S.; Drew, D. *Structure* **2011**, *19*, 17.

(12) Tate, C. G. *Methods Mol. Biol.* **2010**, *601*, 187.

(13) Hovers, J.; Potschies, M.; Polidori, A.; Pucci, B.; Raynal, S.; Bonnete, F.; Serrano-Vega, M. J.; Tate, C. G.; Picot, D.; Pierre, Y.; Popot, J. L.; Nehme, R.; Bidet, M.; Mus-Veteau, I.; Busskamp, H.; Jung, K. H.; Marx, A.; Timmins, P. A.; Welte, W. *Mol. Membr. Biol.* **2011**, *28*, 171.

(14) Lee, S. C.; Bennett, B. C.; Hong, W. X.; Fu, Y.; Baker, K. A.; Marcoux, J.; Robinson, C. V.; Ward, A. B.; Halpert, J. R.; Stevens, R. C.; Stout, C. D.; Yeager, M. J.; Zhang, Q. *Proc. Natl. Acad. Sci. U. S. A.* **2013**, *110*, E1203.

(15) Chae, P. S.; Rasmussen, S. G.; Rana, R. R.; Gotfryd, K.; Chandra, R.; Goren, M. A.; Kruse, A. C.; Nurva, S.; Loland, C. J.; Pierre, Y.; Drew, D.; Popot, J. L.; Picot, D.; Fox, B. G.; Guan, L.; Gether, U.; Byrne, B.; Kobilka, B.; Gellman, S. H. *Nat. Methods* **2010**, *7*, 1003.

(16) Zhou, Y.; Bowie, J. U. *J. Biol. Chem.* **2000**, *275*, 6975.

(17) Miller, J. L.; Tate, C. G. *J. Mol. Biol.* **2011**, *413*, 628.

(18) Popot, J. L. *Annu. Rev. Biochem.* **2010**, *79*, 737.

(19) Di Bartolo, N.; Compton, E. L.; Warne, T.; Edwards, P. C.; Tate, C. G.; Schertler, G. F.; Booth, P. J. *PLoS One* **2016**, *11*, e0151582.

(20) Rouse, S. L.; Sansom, M. S. *J. Phys. Chem. B* **2015**, *119*, 764.

(21) Cheng, X.; Jo, S.; Lee, H. S.; Klauda, J. B.; Im, W. *J. Chem. Inf. Model.* **2013**, *53*, 2171.

(22) O'Mara, M. L.; Mark, A. E. *J. Chem. Theory Comput.* **2012**, *8*, 3964.

(23) Rodriguez-Ropero, F.; Fioroni, M. *J. Struct. Biol.* **2012**, *177*, 291.

(24) Choutko, A.; Glattli, A.; Fernandez, C.; Hilty, C.; Wuthrich, K.; van Gunsteren, W. F. *Eur. Biophys. J.* **2011**, *40*, 39.

(25) Cuthbertson, J. M.; Bond, P. J.; Sansom, M. S. *Biochemistry* **2006**, *45*, 14298.

(26) Patargias, G.; Bond, P. J.; Deol, S. S.; Sansom, M. S. *J. Phys. Chem. B* **2005**, *109*, 575.

(27) Cheng, X.; Im, W. *Biophys. J.* **2012**, *102*, L27.

(28) Stolzenberg, S.; Michino, M.; LeVine, M. V.; Weinstein, H.; Shi, L. *Biochim. Biophys. Acta, Biomembr.* **2016**, *1858*, 1652.

(29) Awoonor-Williams, E.; Rowley, C. N. *Biochim. Biophys. Acta, Biomembr.* **2016**, *1858*, 1672.

(30) Furini, S.; Domene, C. *Biochim. Biophys. Acta, Biomembr.* **2016**, *1858*, 1733.

(31) Pavlova, A.; Hwang, H.; Lundquist, K.; Balusek, C.; Gumbart, J. C. *Biochim. Biophys. Acta, Biomembr.* **2016**, *1858*, 1753.

DOI: 10.1021/jacs.6b08742
J. Am. Chem. Soc. 2016, 138, 15425−15433

(32) Lee, S.; Bhattacharya, S.; Grisshammer, R.; Tate, C.; Vaidehi, N. *J. Phys. Chem. B* **2014**, *118*, 3355.
(33) Keranen, H.; Gutierrez-de-Teran, H.; Aqvist, J. *PLoS One* **2014**, *9*, e108492.
(34) Massink, A.; Gutierrez-de-Teran, H.; Lenselink, E. B.; Ortiz Zacarias, N. V.; Xia, L.; Heitman, L. H.; Katritch, V.; Stevens, R. C.; IJzerman, A. P. *Mol. Pharmacol.* **2015**, *87*, 305.
(35) Robertson, N.; Jazayeri, A.; Errey, J.; Baig, A.; Hurrell, E.; Zhukov, A.; Langmead, C. J.; Weir, M.; Marshall, F. H. *Neuropharmacology* **2011**, *60*, 36.
(36) Lebon, G.; Bennett, K.; Jazayeri, A.; Tate, C. G. *J. Mol. Biol.* **2011**, *409*, 298.
(37) Magnani, F.; Shibata, Y.; Serrano-Vega, M. J.; Tate, C. G. *Proc. Natl. Acad. Sci. U. S. A.* **2008**, *105*, 10744.
(38) Lebon, G.; Warne, T.; Edwards, P. C.; Bennett, K.; Langmead, C. J.; Leslie, A. G.; Tate, C. G. *Nature* **2011**, *474*, 521.
(39) Dore, A. S.; Robertson, N.; Errey, J. C.; Ng, I.; Hollenstein, K.; Tehan, B.; Hurrell, E.; Bennett, K.; Congreve, M.; Magnani, F.; Tate, C. G.; Weir, M.; Marshall, F. H. *Structure* **2011**, *19*, 1283.
(40) Xu, F.; Wu, H.; Katritch, V.; Han, G. W.; Jacobson, K. A.; Gao, Z. G.; Cherezov, V.; Stevens, R. C. *Science* **2011**, *332*, 322.
(41) Liu, W.; Chun, E.; Thompson, A. A.; Chubukov, P.; Xu, F.; Katritch, V.; Han, G. W.; Roth, C. B.; Heitman, L. H.; IJzerman, A. P.; Cherezov, V.; Stevens, R. C. *Science* **2012**, *337*, 232.
(42) Hino, T.; Arakawa, T.; Iwanari, H.; Yurugi-Kobayashi, T.; Ikeda-Suno, C.; Nakada-Nakura, Y.; Kusano-Arai, O.; Weyand, S.; Shimamura, T.; Nomura, N.; Cameron, A. D.; Kobayashi, T.; Hamakubo, T.; Iwata, S.; Murata, T. *Nature* **2012**, *482*, 237.
(43) Dupuy, C.; Auvray, X.; Petipas, C.; et al. *Langmuir* **1997**, *13*, 3965.
(44) Lipfert, J.; Columbus, L.; Chu, V. B.; Lesley, S. A.; Doniach, S. *J. Phys. Chem. B* **2007**, *111*, 12427.
(45) Oliver, R. C.; Lipfert, J.; Fox, D. A.; Lo, R. H.; Doniach, S.; Columbus, L. *PLoS One* **2013**, *8*, e62488.
(46) Warne, T.; Serrano-Vega, M. J.; Tate, C. G.; Schertler, G. F. *Protein Expression Purif.* **2009**, *65*, 204.
(47) Friesen, R. H.; Knol, J.; Poolman, B. *J. Biol. Chem.* **2000**, *275*, 40658.
(48) Butler, P. J.; Ubarretxena-Belandia, I.; Warne, T.; Tate, C. G. *J. Mol. Biol.* **2004**, *340*, 797.
(49) Bamber, L.; Harding, M.; Butler, P. J.; Kunji, E. R. *Proc. Natl. Acad. Sci. U. S. A.* **2006**, *103*, 16224.
(50) Blakey, D.; Leech, A.; Thomas, G. H.; Coutts, G.; Findlay, K.; Merrick, M. *Biochem. J.* **2002**, *364*, 527.
(51) Kawate, T.; Gouaux, E. *Structure* **2006**, *14*, 673.
(52) Gutmann, D. A.; Mizohata, E.; Newstead, S.; Ferrandon, S.; Henderson, P. J.; van Veen, H. W.; Byrne, B. *Protein Sci.* **2007**, *16*, 1422.
(53) Zhang, X.; Stevens, R. C.; Xu, F. *Trends Biochem. Sci.* **2015**, *40*, 79.
(54) Mahmood, I.; Liu, X.; Neya, S.; Hoshino, T. *Chem. Pharm. Bull.* **2013**, *61*, 426.
(55) Weiss, H. M.; Grisshammer, R. *Eur. J. Biochem.* **2002**, *269*, 82.
(56) Warne, T.; Moukhametzianov, R.; Baker, J. G.; Nehme, R.; Edwards, P. C.; Leslie, A. G.; Schertler, G. F.; Tate, C. G. *Nature* **2011**, *469*, 241.
(57) Cherezov, V.; Rosenbaum, D. M.; Hanson, M. A.; Rasmussen, S. G.; Thian, F. S.; Kobilka, T. S.; Choi, H. J.; Kuhn, P.; Weis, W. I.; Kobilka, B. K.; Stevens, R. C. *Science* **2007**, *318*, 1258.
(58) Hanson, M. A.; Cherezov, V.; Griffith, M. T.; Roth, C. B.; Jaakola, V. P.; Chien, E. Y.; Velasquez, J.; Kuhn, P.; Stevens, R. C. *Structure* **2008**, *16*, 897.
(59) Lee, A. G. *Biochim. Biophys. Acta, Biomembr.* **2004**, *1666*, 62.
(60) Moraes, I.; Evans, G.; Sanchez-Weatherby, J.; Newstead, S.; Stewart, P. D. *Biochim. Biophys. Acta, Biomembr.* **2014**, *1838*, 78.
(61) Muller, C. E.; Jacobson, K. A. *Biochim. Biophys. Acta, Biomembr.* **2011**, *1808*, 1290.
(62) Bill, R. M.; Henderson, P. J.; Iwata, S.; Kunji, E. R.; Michel, H.; Neutze, R.; Newstead, S.; Poolman, B.; Tate, C. G.; Vogel, H. *Nat. Biotechnol.* **2011**, *29*, 335.
(63) Carpenter, B.; Nehme, R.; Warne, T.; Leslie, A. G.; Tate, C. G. *Nature* **2016**, *536*, 104.
(64) Miller-Gallacher, J. L.; Nehme, R.; Warne, T.; Edwards, P. C.; Schertler, G. F.; Leslie, A. G.; Tate, C. G. *PLoS One* **2014**, *9*, e92727.
(65) Griffin, W. C. *J. Soc. Cosmet. Chem.* **1954**, *5*, 245.
(66) Hess, B.; Kutzner, C.; van der Spoel, D.; Lindahl, E. *J. Chem. Theory Comput.* **2008**, *4*, 435.
(67) Oostenbrink, C.; Villa, A.; Mark, A. E.; van Gunsteren, W. F. *J. Comput. Chem.* **2004**, *25*, 1656.
(68) Ballesteros, J. A.; Weinstein, H. In *Methods in Neurosciences*; Stuart, C. S., Ed.; Academic Press: San Diego, CA, 1995; Vol. *25*, p 366.
(69) Berendsen, H. J.; Postma, J. P.; van Gunsteren, W. F.; Hermans, J. In *Intermolecular Forces*; Pullman, B., Ed.; D. Reidel Publishing Company: Dordrecht, the Netherlands, 1981; p 331.
(70) Manglik, A.; Kim, T. H.; Masureel, M.; Altenbach, C.; Yang, Z.; Hilger, D.; Lerch, M. T.; Kobilka, T. S.; Thian, F. S.; Hubbell, W. L.; Prosser, R. S.; Kobilka, B. K. *Cell* **2015**, *161*, 1101.
(71) Kuszak, A. J.; Pitchiaya, S.; Anand, J. P.; Mosberg, H. I.; Walter, N. G.; Sunahara, R. K. *J. Biol. Chem.* **2009**, *284*, 26732.
(72) Berendsen, H. J.; Postma, J. P.; van Gunsteren, W. F.; Di Nola, A.; Haak, J. R. *J. Chem. Phys.* **1984**, *81*, 3684.
(73) Ryckaert, J. P.; Ciccotti, G.; Berendsen, H. J. *J. Comput. Phys.* **1977**, *23*, 327.
(74) Scott, W. R. P.; et al. *J. Phys. Chem. A* **1999**, *103*, 3596.
(75) Miyamoto, S.; Kollman, P. A. *J. Comput. Chem.* **1992**, *13*, 952.
(76) Hess, B.; Bekker, H.; Berendsen, H. J.; Fraaije, J. G. *J. Comput. Chem.* **1997**, *18*, 1463.
(77) Darden, T.; York, D.; Pedersen, L. *J. Chem. Phys.* **1993**, *98*, 10089.
(78) Essmann, U.; Perera, L.; Berkowitz, M. L.; Darden, T.; Lee, H.; Pedersen, L. G. *J. Chem. Phys.* **1995**, *103*, 8577.

DOI: 10.1021/jacs.6b08742
J. Am. Chem. Soc. 2016, 138, 15425−15433